Journal of Materials Chemistry C

Accepted Manuscript

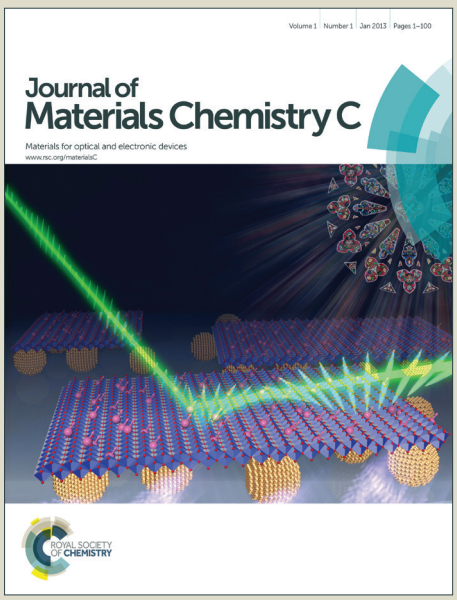

ROYAL SOCIETY OF CHEMISTRY

www.rsc.org/materialsC

Oxadiazole based bipolar host materials employing planarized triarylamine donors for RGB PHOLEDs with low efficiency roll-off†

Paul Kautny,[a] Daniel Lumpi,*[a] Yanping Wang,[b] Antoine Tissot,[c]

Johannes Bintinger,[a] Ernst Horkel,[a] Berthold Stöger,[d] Christian Hametner,[a]

Hans Hagemann,[c] Dongge Ma,[b] and Johannes Fröhlich[a]

[a] Institute of Applied Synthetic Chemistry, Vienna University of Technology, Getreidemarkt 9/163, A-1060 Vienna, Austria

[b] State Key Laboratory of Polymer Physics and Chemistry, Changchun Institute of Applied Chemistry, Chinese Academy of Sciences, Changchun, 130022, China

[c] Département de Chimie Physique, Université de Genève, 30, quai E. Ansermet, 1211 Geneva 4, Switzerland

[d] Institute of Chemical Technologies and Analytics, Vienna University of Technology, Getreidemarkt 9/164, A-1060 Vienna, Austria

daniel.lumpi@tuwien.ac.at

† Electronic supplementary information (ESI) available: NMR spectra, TGA/DSC analyses, cyclic voltammetry, phosphorescence as well as electroluminescence spectra, DFT calculations and crystallographic information; See DOI:

Abstract

A series of 6 novel triarylamine-containing oxadiazole compounds (**o-PCzPOXD**, **o-ICzPOXD**, **o-TPATOXD**, **o-PCzTOXD**, **o-ICzTOXD**, **o-CzTOXD**) have been designed, synthesized and characterized concerning applications as host materials in PHOLED devices. To further improve the *ortho*-linkage concept, the impact of incorporating planarized electron-donating triarylamine (TAA) structures on intramolecular charge transfer was examined. The effect was evaluated for two series of electron-accepting oxadiazole scaffolds, realizing *ortho*-linkage on the benzene (POXD) and the thiophene (TOXD) core. Thermal analysis shows increased glass-transition temperatures for planarized structures indicating an improved morphological stability. A higher degree of planarization also results in significantly increased singlet and triplet energy values, revealing the impact on the intramolecular charge transfer. Employing the developed materials, red (**o-TPATOXD**: CE_{max}: 28.8 cd A^{-1}, EQE_{max}: 16.9%), green (**o-PCzPOXD**: CE_{max}: 62.9 cd A^{-1}, EQE_{max}: 17.1%) and blue (**o-PCzPOXD**: CE_{max}: 29.8 cd A^{-1}, EQE_{max}: 13.4%) devices were achieved showing remarkably low efficiency roll-off for planarized donors. Hence, this is the first report of efficient blue devices for this specific class of host materials. It is proposed that the results correlate with an increasing *ortho*-linkage effect and decreasing donor strength of the TAA moiety by planarization and, thus, tackling one of the major challenges in PHOLED research: improving both triplet energy and compound stability.

Table of Content

Graphic:

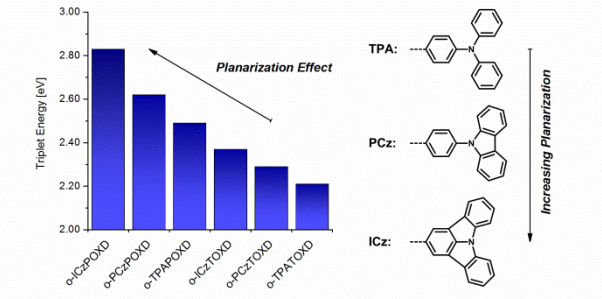

Text:

The significant impact of the planarization of triarylamine donor structures on thermal, photo-physical and electro-chemical properties of novel host materials is examined with regard to PHOLED applications.

Introduction

Organic Light Emitting Diodes (OLEDs) and their application in display technology represent the most advanced technology among the rapidly growing field of organic electronics.[1-7] Since the groundbreaking work of Forrest et al. from 1998[8,9] great efforts have been made in developing Phosphorescent Organic Light Emitting Diodes (PHOLEDs) typically employing heavy transition metal complexes.[10,11] In contrast to fluorescent OLEDs phosphorescent emitters are capable of harvesting triplet and singlet excitons simultaneously and, thus, can theoretically achieve 100% internal quantum efficiency.[12,13]

However, high concentration of triplet excitons leads to triplet-triplet annihilation at high current rates resulting in efficiency roll-off.[14] Thus, phosphorescent emitters are generally widely dispersed in an organic host material. Efficient host materials have to fulfill some basic requirements:[7] (i) higher triplet energy (E_t) value than the dopant to effectively confine triplet excitons on the phosphorescent emitter; (ii) suitable HOMO / LUMO levels to facilitate charge injection; (iii) morphological stability for durable and long lasting devices.

Bipolar host materials received great attention in recent years, due to their balanced charge transport properties resulting in broad charge recombination zones. However, combining donor and acceptor subunits in one molecule ultimately lowers the E_t as a result of the intramolecular charge transfer.[7] Therefore, the molecular design of bipolar host materials focuses on the interruption of the conjugated π-system in order to reduce donor-acceptor interactions and thus to retain high E_t values. Among the most efficient ways to separate the molecular subunits is the introduction of specific linkage modes.[7] Particularly, *ortho*-linkage of donor and acceptor subunits, inducing

twisted molecular conformations, proved to be a highly efficient strategy to achieve large triplet bandgap materials.[15]

In this contribution we reveal the enhancement of the effect of *ortho*-linkage by applying increasingly planarized triarylamine donors (from *N*,*N*-diphenylbenzenamin (TPA) to 9-phenyl-9*H*-carbazole (PCz) and indolo[3,2,1-*jk*]carbazole (ICz)) to an established phenyl-oxadiazole-phenyl (POXD) acceptor. The corresponding triphenylamine compound (**o-TPAPOXD**) has been previously demonstrated to be highly efficient as host in red and green PHOLED devices.[16,17] Utilizing the planarized arylamines we were able to increase singlet as well as triplet energies resulting in higher efficiencies and significantly reduced efficiency roll-off in non-optimized red, green and blue PHOLED devices. We propose that these findings correlate with an increasing *ortho*-linkage effect due to steric impact and decreasing donor strength of the triarylamine moiety by planarization as a result of the contribution of the nitrogen lone-pair to the aromaticity of the formed pyrrole subunit(s). To prove the developed concept, TPA, PCz, ICz as well as carbazole (Cz) donors were also applied to a new thiophene-oxadiazole-thiophene (TOXD) acceptor motive confirming the trends.

Employing the developed materials red (**o-TPATOXD**: CE_{max}: 28.7 cd A^{-1}, EQE_{max}: 16.9%), green (**o-PCzPOXD**: CE_{max}: 62.9 cd A^{-1}, EQE_{max}: 17.1%) and blue (**o-PCzPOXD**: CE_{max}: 29.8 cd A^{-1}, EQE_{max}: 13.4%) devices have been obtained.

Hence, we report on an efficient approach to gain control of intramolecular charge transfer, significantly affecting singlet as well as triplet energies, by the planarization of electron donating triarylamine moieties. As a result, novel host materials have been designed, synthesized and characterized exhibiting remarkably low efficiency roll-off, which is of technological relevance for both single doped devices and multi-color based white PHOLEDs.

Results and Discussion

Synthesis

The synthesis of target host materials and precursors primarily relies on organo-lithium assisted and transition-metal catalyzed (Ullman condensation, Suzuki cross-coupling) reactions. The first part describes the synthetic pathways towards planarized triarylamine (TAA) structures phenylcarbazole and indolocarbazole particularly focusing on C-H activation as an efficient approach to acquire the desired planarization. In the second part the realization of the *ortho*-linkage on the benzene (**5a-c**) core and subsequently the thiophene core (**8a-d**), achieved *via* a Halogen Dance (HD) reaction, is outlined.

Boronic esters of triphenylamine (**3a**) and phenylcarbazole (**3b**) were obtained in analogy to literature.[18-20] The synthesis of indolocarbazole boronic ester (**3c**) is based on a recently developed methodology utilizing C-H activation.[21] Compared to previously reported procedures this synthetic approach towards indolo[3,2,1-*jk*]carbazole **2** (Scheme 1) is shorter (less steps), more efficient and does not rely on the application of special equipment (e.g. vacuum flash pyrolysis).[22,23] Although good yields of 83% (15 mol% $Pd(OAc)_2$ catalyst) were accomplished the reduction of catalyst loads drastically decreases the reaction conversion. The use of 5 mol% $Pd(OAc)_2$ even limits the product formation to trace amounts.[21] Hence, we report on an improved procedure at significantly reduced catalyst amounts (2 mol%) towards indolo[3,2,1-*jk*]carbazole employing $Pd(PPh_3)_4$ and K_2CO_3 (71% yield). In fact, the application of (NHC)Pd(allyl)Cl[24,25] catalyst (2 mol%) further improves the yields to 94% (Scheme 1 and Table 1). Moreover, the substrate scope could be broadened to chlorine derivatives (no conversion for $Pd(PPh_3)_4$, Table 1).

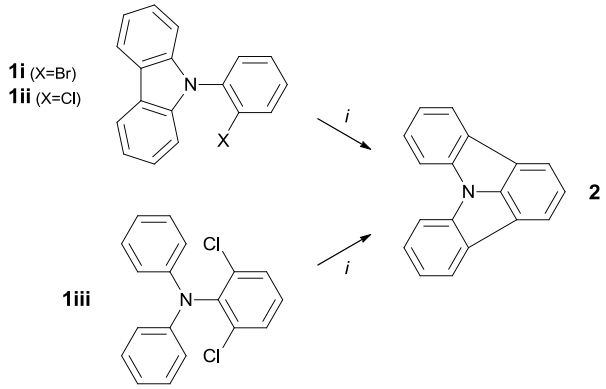

Scheme 1 Synthetic pathways towards indolo[3,2,1-*jk*]carbazole **2**; *i*: (NHC)Pd(allyl)Cl (2 mol%), K_2CO_3 (2.0 eq.), DMA (0.2 M), 130 °C, 1-2h.

Table 1 Results of the C-H activation for substrates **1i-iii**.

Substrate	$Pd(PPh_3)_4$	(NHC)Pd(allyl)Cl
1i	71%[a]	94%[a]
1ii	n.c.[b]	94%[a]
1iii	n.c.[b]	80%[a]

[a]Isolated yields. [b]No conversion (GC-MS).

Particularly, the demonstrated two-fold C-H activation of chlorine derivatives allows for a convenient and selective synthesis of a variety of novel target structures, broadening the scope of accessible indolo[3,2,1-*jk*]carbazole motives.

Selective bromination (NBS, 54%)[23] of **2** and organo-lithium assisted transformation (*n*-BuLi, isopropyl pinacol borate, 69%) yielded the indolocarbazole pinacol boronic ester **3c**. The crystal structure (see ESI† for details) discloses the desired planarity of this TAA type structure. **3c**[26] crystallizes with one crystallographically unique molecule in the asymmetric unit located on a general position. The aromatic system is close to flat: The N atom is located 0.1573(5) Å from the least squares (LS) plane defined by the C atoms of the benzene rings.

The dibrominated POXD (benzene – oxadiazole – benzene structure) precursor **4** was synthesized according to literature.[27] The conversion towards target compounds

5a-c was accomplished utilizing TAA boronic esters **3a-c** applying a standard Suzuki protocol (Scheme 2).[28] Good to excellent yields of 85% and 93% were achieved for **5a** and **5b**, respectively; the lower yield for **5c** (39%) is attributed to a lower solubility affecting both reaction conversion and work-up.

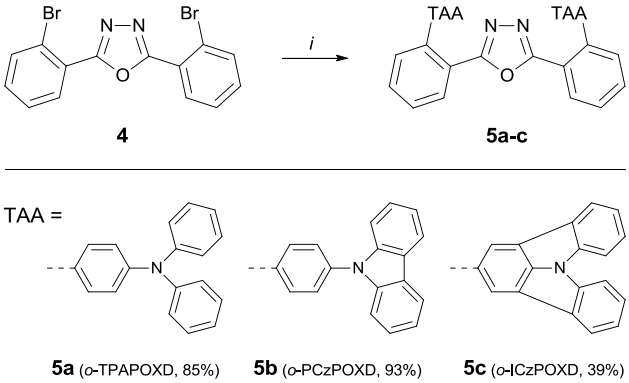

Scheme 2 Synthesis of POXD based host materials **5a-c**; *i*: boronic acid ester **3a-c** (2.5 eq.), K_2CO_3 (5.0 eq., 2 M aq.), $Pd(PPh_3)_4$ (5 mol%), THF (~0.5 M), reflux.

In contrast to the POXD series the dibrominated TOXD (thiophene – oxadiazole – thiophene structure), precursor **7i** is unknown to literature. The *ortho*-substitution pattern is realized by applying a double-sided Halogen Dance (HD)[29-31] methodology (Scheme 3) starting from **6** (synthesized according to literature). Due to coordinating and activating effects of the oxadiazole moiety[32] the lithium diisopropylamide (LDA) induced metallation selectively takes place in the respective *ortho*-positions. Subsequently, a rearrangement of the bromine atoms (“Halogen Dance”), resulting in the thermodynamically most stable organo-lithium intermediate, yields the desired *ortho*-substitution pattern.

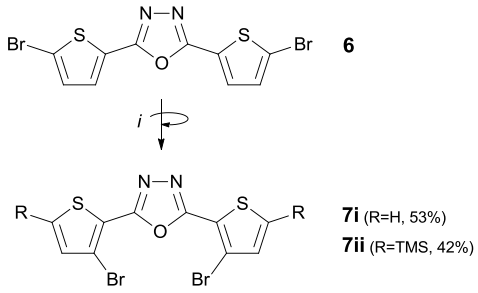

Scheme 3 Halogen Dance reaction towards *ortho*-substitution patterns (**7i-ii**); *i*: THF, -25 °C, LDA (2.4 eq.), 30 min stirring prior to addition of electrophile (MeOH and TMS-Br).

As a consequence, this approach enables to directly introduce substituents R in the 5-positions by addition of suitable electrophiles (R), which has been demonstrated utilizing TMS-Br to yield the silylated compound **7ii**. Hence, specific alterations of material properties e.g. solubility (for e.g. solution processing) can be achieved; however, reaction conditions were not further optimized in this study.

The triarylamine and carbazole cap structures are attached to the TOXD core *via* Suzuki cross-coupling reaction[33-35] and Ullmann condensation,[36-38] respectively (Scheme 4).

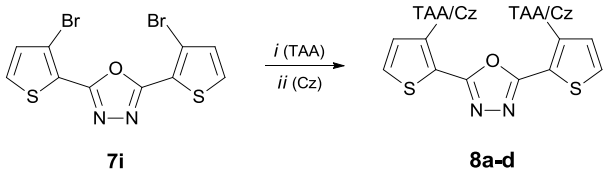

Scheme 4 Synthesis of TOXD based host materials **8a-d**; *i*: Suzuki Cross-Coupling: boronic acid ester **3a**-**c** (3.0 eq.), KO^{t}Bu (3.0 eq.), (NHC)Pd(allyl)Cl (2 mol%), ^{i}PrOH/H_2O (3:1, 5 mM), rf; *ii*: Ullmann condensation: carbazole (3.0 eq.), K_2CO_3 (3.0 eq.) and $CuSO_4 \cdot 5H_2O$ (6.4 mol%), 230 °C.

The Suzuki reaction utilizing TAA precursors **3a-c** was shown to proceed in good to moderate yields using $Pd(PPh_3)_4$. However, improved yields and more reliable results could be obtained by applying (NHC)Pd(allyl)Cl,[24] (55% - 74%) which generally turned out to be a highly efficient catalyst for thiophene-benzene cross-coupling. Attempts of Buchwald-Hartwig reactions in order to introduce the carbazole did not give satisfactory results, which led to a solvent-free Ullmann procedure[20] using $CuSO_4 \cdot 5H_2O$ as catalyst.

Thermal Properties

The thermal stability of the target host materials was investigated by TGA. High decomposition temperatures (T_d – determined from 5% mass loss) between 392 °C and 426 °C were observed for all materials. Glass transition temperatures (T_g) were analyzed by DSC. Whereas **o-TPAPOXD** exhibits glass transition at 94 °C[16] the values for **o-PCzPOXD** (125 °C) and **o-ICzPOXD** (152 °C) are significantly higher indicating improved morphological stability of thin films in PHOLED devices. Within the TOXD series **o-PCzTOXD** also features higher glass transition at 135 °C compared to **o-TPATOXD** (101 °C) or **o-CzTOXD** (106 °C) while no glass transition was detected for **o-ICzTOXD**. In general, the incorporation of the thiophene linker (TOXD derivatives) resulted in slightly higher glass transition temperatures in relation to the corresponding POXD compounds. Higher T_g values for PCz and ICz compounds compared to TPA structure are attributed to an increased rigidity of the TAA moieties. All observed values are distinctly higher compared to CBP (62 °C[7]).

Photo-Physical Properties

Fig. 1 (left) displays the UV/VIS absorption and photoluminescence (PL) spectra of **o-PCzPOXD** and **o-ICzPOXD** as well as "reference compound" **o-TPAPOXD**. Spectra of the TOXD series are depicted in Fig. 1 (right). The optical bandgaps (opt. BG), determined from absorption onsets, are summarized in Table 2.

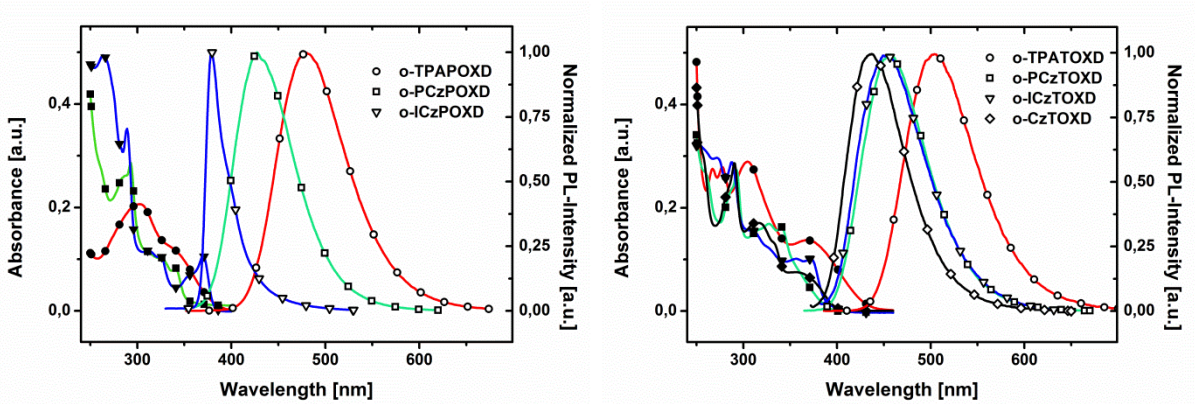

Fig. 1 Absorption (full symbols) and PL (hollow symbols) characteristics of host materials **5a-c** (POXD series, left) and **8a-d** (TOXD series, right); recorded in 5 µM solution in DCM at r.t.

The absorption bands of **o-TPAPOXD** and **o-TPATOXD** at 305 nm are assigned to triphenylamine centered n-π* transition.[39] All carbazole containing compounds exhibit sharp absorption peaks around 290 nm, which are attributed to the n-π* transition of the carbazole moiety.[40] Indolocarbazole containing **o-ICzTOXD** and **o-ICzPOXD** feature a related n-π* transition below 300 nm. Longer wavelength absorption bands result from π-π* charge transfer transitions from electron-donating arylamines to electron-accepting oxadiazole.[41] Strikingly, the absorbance of charge transfer transition is significantly lower for **o-PCzPOXD** and **o-ICzPOXD** compared to **o-PCzTOXD** and **o-ICzTOXD**, indicating that the partial disruption of the conjugated π-system by *ortho*-linkage is more effectively realized on the benzene spacer.

For the TOXD series also a significant blue shift of the absorption onset from **o-TPATOXD** (~450 nm) to **o-PCzTOXD** and **o-ICzTOXD** (both located at ~400 nm) has

been observed, indicating increased optical bands gap as a result of planarized TAA donors.

Photoluminescence (PL) spectroscopy revealed a fluorescence emission maximum of **o-TPAPOXD** located at 479 nm. A significant blue shift of the emission maxima is observed for both **o-PCzPOXD** (428 nm) and **o-ICzPOXD** (379 nm). These results impressively demonstrate the impact of planarizing TAA donors by shifting the singlet emission by up to 100 nm (ΔE = 0.68 eV). Similar trends were observed for the TOXD series (**o-TPATOXD** (502 nm), **o-PCzTOXD** (456 nm) and **o-ICzTOXD** (452 nm)). We propose that these findings correlate with an increasing *ortho*-linkage effect (more twisted conformation) and decreasing donor strength of the TAA moiety (ICz < PCz < TPA) by planarization. The alteration in donor strength is attributed to the fact that the lone pair of the nitrogen is increasingly contributing to the aromaticity (PCz and ICz). **o-CzTOXD** shows an emission maximum at 436 nm; the deep blue emission characteristic is due to the less extended conjugated π-system compared to the TAA structures. Clearly, all POXD compounds exhibit blue shifted emission with respect to the thiophene analogs (TOXD) indicating a more effective donor-acceptor separation for the benzene spacer.

Phosphorescence spectroscopy (77 K) revealed that planarization also impacts triplet emission, although the effect is less pronounced compared to singlet emission. The E_t values, deduced from the highest vibronic sub-band of the phosphorescent spectra, of **o-TPAPOXD**, **o-PCzPOXD** and **o-ICzPOXD** were determined to be 2.49 eV (2.46 eV[16]), 2.62 eV and 2.83 eV, respectively. Compared to the POXD series the E_t values of the TOXD materials **o-TPATOXD** (2.21 eV), **o-PCzTOXD** (2.29 eV), **o-ICzTOXD** (2.37 eV) and **o-CzTOXD** (2.39 eV) are shifted to lower energies.

Although the E_t values significantly increase as a consequence of planarization for both series, host materials of the TOXD series are restricted to low energy emitters. In contrast, the triplet energies of the POXD series are suitable for the construction of green devices.[16,17] E_t values of > 2.60 eV for the PCz and ICz donor structures potentially broaden the scope even to blue phosphorescent emitters (e.g. FIrPic). Particularly the unexpectedly high E_t value (2.83 eV) for **o-ICzPOXD** reveals the effect of incorporating indolo[3,2,1-*jk*]carbazole structures; a possible explanation for these findings is given by DFT calculations (see below).

Additionally, lifetimes for the excited singlet and triplet states were determined. Most striking are the significantly longer triplet lifetimes (τ) found in the POXD series (**o-TPAPOXD** (~790 ms), **o-PCzPOXD** (~335 ms), **o-ICzPOXD** (~349 ms)) compared to the TOXD compounds; triplet lifetimes for the TOXD structures range from 8.2 ms – 12.3 ms. The sulfur atoms in the TOXD compounds are subject to stronger spin-orbit coupling which leads to somewhat relaxed selection rules for transitions between singlet and triplet states (i.e. shorter lifetimes of the triplet). Further details on photo-physical properties are given in the ESI†.

Electro-Chemical Properties

Electro-chemical properties (Table 2) of target materials were investigated by cyclic voltammetry (CV). Predominately determined by electron-rich triarylamines, the HOMO energy levels span in a narrow range of -5.73 eV to -5.64 eV with the exception of **o-TPAPOXD** and **o-TPATOXD** at -5.25 eV[16] and -5.30 eV, respectively. Thus, the incorporation of planarized TAA donors significantly lowers the HOMO energy levels. While **o-TPATOXD** shows reversible oxidation, all carbazole and

indolocarbazole containing materials exhibit irreversible oxidation waves due to the instability of the formed cations.[23,42,43] Quasi reversible reductions were observed during cathodic scans; however, no significant reduction process was observed for **o-ICzPOXD**. The LUMO energy levels of the compounds are located between -2.68 eV and -2.41 eV. These values indicate no significant injection barrier for charge carriers from adjacent charge transporting layers.

Table 1 Physical data of synthesized materials.

	$T_g/T_c/T_m/T_d$ [°C][a]	opt. BG [eV][b,c]	$\lambda_{PL,max}$ [nm][c]	HOMO/LUMO [eV]		E_T (eV)	
				exp.[d]	cal.[e]	exp.[f]	cal.[g]
o-TPAPOXD	94/---/270/432[16]	3.24	479	-5.25/-2.41[16]	-5.14/-1.77	2.49	2.63
o-PCzPOXD	125/n.o.[h]/252/395	3.51	428	-5.64/-2.50	-5.55/-2.04	2.62	2.83
o-ICzPOXD	152/231/308/404	3.26	379	-5.73/-2.50[i]	-5.70/-1.84	2.83	2.88
o-TPATOXD	101/n.o.[h]/184/414	2.88	502	-5.30/-2.57	-5.19/-2.11	2.21	2.21
o-PCzTOXD	135/n.o.[h]/261/426	3.19	456	-5.66/-2.68	-5.57/-2.37	2.29	2.30
o-ICzTOXD	n.o.[h]/302/341/402	3.19	452	-5.68/-2.56	-5.70/-2.03	2.37	2.36
o-CzTOXD	106/n.o.[h]/211/392	3.11	436	-5.69/-2.66	-5.65/-2.39	2.39	2.33

[a]Determined from TGA / DSC analysis; T_c: crystallization temperature. [b]Estimated from the absorption onset. [c]Measurement in DCM (5 µM) at r.t. [d]Calculated from onsets of oxidation and reduction peaks. [e]Calculated applying density functional theory level (B3LYP/6-311+G*). [f]Estimated from the highest energy vibronic transition in toluene at 77 K. [g]Calculated applying time-dependent density functional theory level (B3LYP/6-311+G*). [h]Not observed. [i]Calculated from HOMO level and absorption onset.

Theoretical Calculations

To investigate the geometrical and electronic properties of the target compounds at molecular level studies applying density functional theory (DFT) and time-dependent DFT (TDDFT) calculations were conducted (for additional details see Experimental Section). According to DFT calculations, absolute HOMO / LUMO values are in the range of 5.14 eV – 5.70 eV / 1.77 eV – 2.39 eV, which correlates with the experimental data; LUMO levels show a systematic shift of ~0.5 eV.

The contour plots for **5a** and **8a**, comparing the POXD with the corresponding TOXD compounds, are depicted in Fig. 2. As expected, HOMO levels are mainly located at one of the TAA structures and the LUMOs at the oxadiazole containing cores (POXD and TOXD). This separation, particularly crucial for high triplet energies, was found to be more efficiently realized for the POXD series (benzene linker) for all substance pairs, which is in agreement with photo-physical data (Table 2). Inspecting the TPA (Fig. 2 (left)) and PCz (Fig. 3 (left)) scaffolds a similar trend is being observed: A reduced HOMO / LUMO overlap is indicated for the more rigidified PCz versus the TPA structures. The comparison of the average tilting angles of the of POXD and the TOXD benzene to the TAA benzene core supports the aforementioned assumptions: 54.6° (56.2° / 53.0°) **o-TPAPOXD** < 58.7° (62.2° / 55.2°) **o-PCzPOXD** < 59.7° (61.9° / 57.5°) **o-ICzPOXD** and 50.2° (52.0° / 48.3°) **o-TPATOXD** < 54.3° (57.8° / 50.8°) **o-PCzTOXD** < 54.9° (57.0° / 52.8°) **o-ICzTOXD** (the exact tilting angle values for each side of the unsymmetric molecules are given in brackets).

A remarkable result of the calculation was acquired for **o-ICzPOXD** (Fig. 3 (right)). Whereas the HOMO is positioned at the TAA (ICz) scaffold (as expected), the LUMO is not located on the POXD core but on the opposed ICz moiety. Potentially, this fact is an explanation for the aforementioned unexpectedly high triplet energy observed as a result of the enhanced spatial separation and modified acceptor properties. This finding outlines the significant deviation in donor strength for the applied TAA structures and the effect on material properties. In contrast, the LUMO in the **o-ICzTOXD** remains located at the TOXD core (as observed for all other molecules), which corresponds to the detected triplet and singlet energy value relations; thus, supports the hypothesis for the LUMO located on the ICz core in **o-ICzPOXD**.

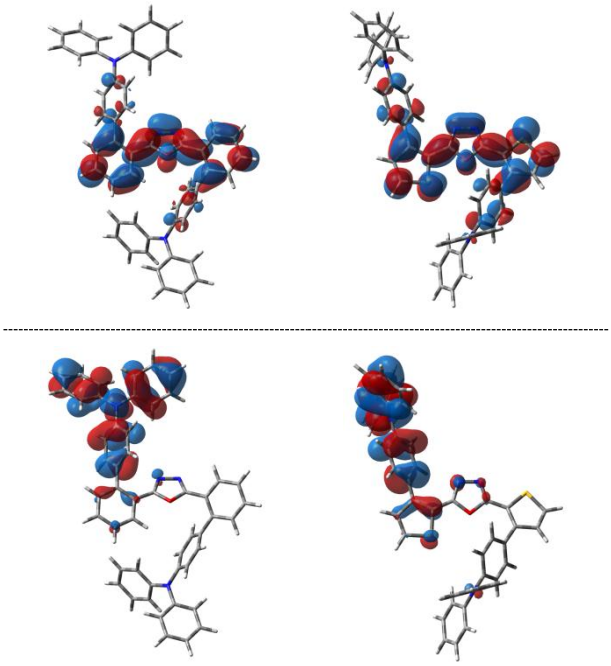

Fig. 2 HOMO (bottom) and LUMO (top) of **o-TPAPOXD** (left) and **o-TPATOXD** (right).

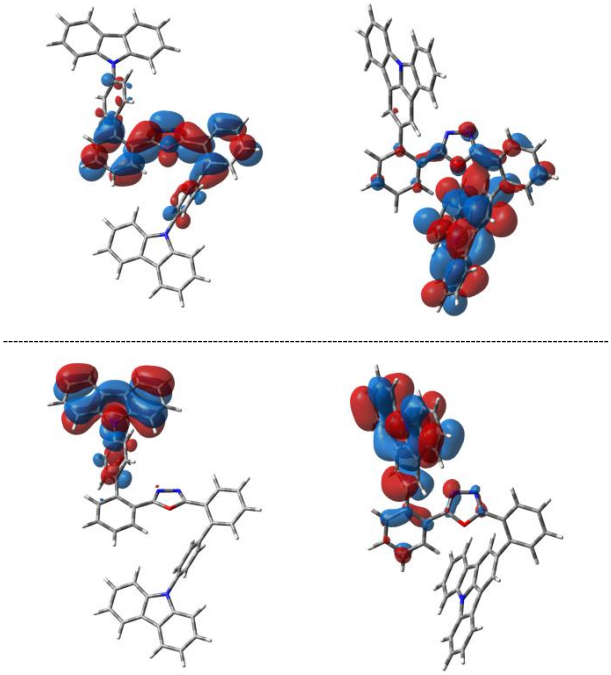

Fig. 3 HOMO (bottom) and LUMO (top) of **o-PCzPOXD** (left) and **o-ICzPOXD** (right).

Crystallography

o-PCzPOXD (**5b**)[44] (Fig. 4 (left)) crystallizes with one crystallographically unique molecule in the asymmetric unit. The molecules are pseudo-symmetric by twofold rotation around an axis passing through the O atom of the oxadiazole ring. The PCz donor units are located on the side of the O atom of the oxadiazole ring. Due to steric interaction of these groups, the core benzenes (POXD) are strongly inclined to each other (angle between the LS planes 60.95(3)°) and to the central oxadiazole ring (32.45(8)° and 33.64(8)°). The carbazole moieties are moderately inclined with respect to the core benzenes (15.58(9)° and 16.25(9)°). On the other hand the PCz-benzene rings are distinctly inclined to the POXD benzenes (53.49(6)° and 54.12(6)°) and carbazoles (56.38(5)° and 57.68(5)°).

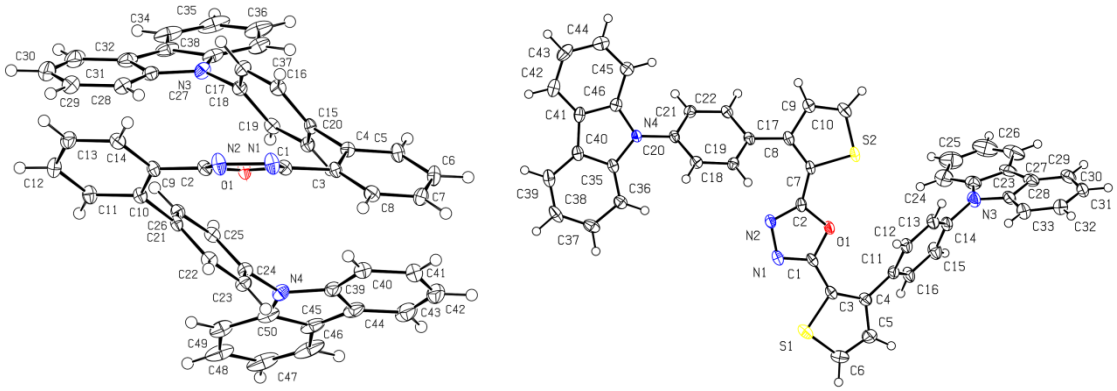

Fig. 4 Molecular structures of **o-PCzPOXD** (left) and **o-PCzTOXD** (right) – C, N, O and S atoms are represented by white, blue, red and yellow ellipsoids drawn at 50% probability levels, H atoms by spheres of arbitrary radius. For **o-PCzTOXD** only one out of two unique molecules is shown.

o-PCzTOXD (**8b**)[45] (Fig. 4, (right)) crystallizes with two crystallographically different molecules (*Z*' = 2) located on general positions. Both molecules are geometrically virtually equivalent. One thiophene ring is in *trans*- and one in *cis*-conformation with respect to the central oxadiazole ring. Thus, both PCz moieties face opposite directions. This is in contrast to the crystal structures of **o-PCzPOXD** and the solvates of the thiadiazole analog of **o-PCzTOXD** (as reported in earlier studies), in

which the thiadiazole and thiophene rings are all in *trans*- and, therefore, the PCz units in *cis*-conformation.[46] The thiophene and oxadiazole rings in *cis*-conformation are practically planar with tilt angles of 3.17(10)° and 3.53(10)°. In contrast, the thiophenes in the *trans*-conformation feature distinct inclination to the oxadiazole ring (12.03(11)° and 11.44(11)°). Whereas the carbazole connected *via* the PCz-benzene to the *cis*-located thiophene is nearly coplanar with the latter (3.17(8)°, 2.33(8)°), the *trans*-located thiophene is strongly inclined to the corresponding carbazole (76.91(9)°, 76.86(9)°). The PCz-benzenes on the other hand are, like in **o-PCzPOXD**, always strongly inclined to the neighboring aromatic moieties (tilt angles to thiophene: 45.82(10)° – 47.93(10)°; to carbazoles: 44.59(8)° – 61.06(8)°).

Charge Transport Properties

In order to study the influence of the four investigated arylamine-donors on charge transport properties within the **TOXD** series, hole-only devices (HODs; structure: ITO / MoO_3 (8 nm) / Host (80 nm) / MoO_3 (8 nm) / Al) and electron-only devices (EODs; structure: Al / Li_2CO_3 (1 nm) / Be:Li_2CO_3 (30 nm) / Host (80 nm) / Be:Li_2CO_3 (30 nm) / Li_2CO_3 (1 nm) / Al) were fabricated. It is noted that the HOMO levels of **o-CzTOXD**, **o-PCzTOXD** and **o-ICzTOXD** are nearly 0.4 eV lower compared to **o-TPATOXD**. This fact may hamper hole injection to the HODs, however, displays the actual situation in the PHOLED devices. Current-voltage curves are given in Fig. 5.

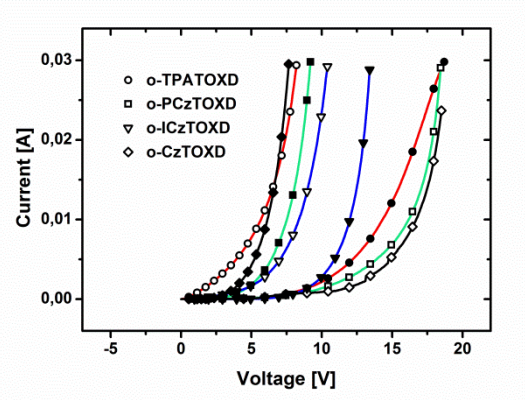

Fig. 5 Current–voltage (I–V) curves of hole- (hollow symbols) and electron-only (full symbols) devices.

o-TPATOXD exhibits good hole transport properties due to the presence of the triphenylamine moiety; significantly lower current density was observed in the EOD. In contrast carbazole based **o-CzTOXD** and **o-PCzTOXD** feature better electron transport properties. While **o-PCzTOXD** exhibits similarly low hole current density compared to **o-CzTOXD**, the current density in the EOD applying **o-PCzTOXD** is lower and therefore charge transport in **o-PCzTOXD** is more balanced than in **o-CzTOXD**. For **o-ICzTOXD** the HOD shows higher current density than the EOD. Furthermore, carrier properties in **o-ICzTOXD** are more balanced compared to the other host materials. Thus, the incorporation of the indolocarbazole moiety resulted in the most bipolar character of **o-ICzTOXD** among this series of materials. The same trends were found for the **POXD** series with the exception of the EOD of **o-ICzPOXD** featuring hardly any electron transport. This finding can be explained by the significantly altered orbital distribution of **o-ICzPOXD** as discussed in the theoretical part.

Electroluminescent Properties

To evaluate the applicability of the POXD series as universal host materials for RGB PHOLED devices with a standard architecture of ITO / MoO_3 (8 nm) / NPB (50 nm) / TCTA (5 nm) / EML (10 nm) / TPBI (25 nm) / LiF(1 nm) / Al, in which the EMLs consist of coevaporated hosts **o-TPAPOXD** (**I**), **o-PCzPOXD** (**II**) or **o-ICzPOXD** (**III**) and guest $Ir(MDQ)_2(acac)$ (**R**), $Ir(ppy)_3$ (**G**) or FIrPic (**B**), were fabricated. NPB is used as hole transporting layer while TPBI is applied as electron transporting and hole blocking layer due to its low lying HOMO level.[47-50] Additionally a thin TCTA layer is inserted between the hole transporting and emitting layer in order to confine triplet excitons more effectively in the EML as result of a larger triplet energy of TCTA compared to NPB.[48] The standard device architecture including HOMO and LUMO levels of all employed materials is depicted in Fig. 6.

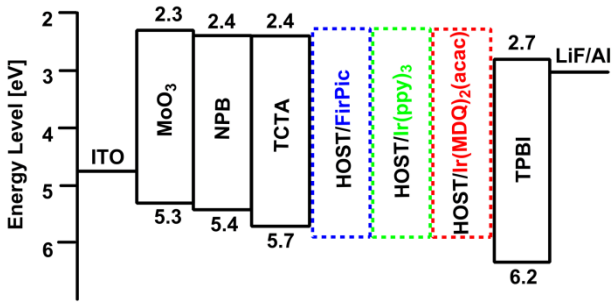

Fig. 6 Schematic energy level diagram of the device architecture employed in this work.

Current density-voltage-luminance and current efficiency-luminance-power efficiency curves for all devices are depicted in Fig. 7 and the electroluminescent properties of all fabricated PHOLED devices are summarized in Table 3. Among green devices the best efficiency was achieved for device **GII** (host material: **o-PCzPOXD**), giving a maximum current efficiency (CE) of 62.9 cd A^{-1}, a maximum power efficiency (PE) of 53.5 lm W^{-1} and a maximum external quantum efficiency (EQE) of 17.1%, while lower values were obtained for **GI** and **GIII** with CE_{max} of 35.1 cd $A^{-1}$and 48.8 cd A^{-1}, PE_{max}

of 34.4 lm W^{-1} and 51.6 lm W^{-1} and EQE_{max} of 10.3% and 13.8%, respectively. We emphasize that significantly higher efficiencies were obtained by applying **o-PCzPOXD** and **o-ICzPOXD** in our standard device configuration compared to **o-TPAPOXD**. In fact, using **o-TPAPOXD** Tao et al.[17] reported highly efficient green PHOLED devices reaching EQE_{max} of 22.0% (vs. EQE_{max} of 10.3%) after optimization of device architecture, thus revealing the potential of the newly developed materials within this paper. Notably, at illumination relevant brightness of 1000 cd m^{-2} devices **GII** and **GIII** retained high CE of 61.2 cd $A^{-1}$and 48.1 cd A^{-1}. These values correspond to remarkably low efficiency roll-offs of 2.7 and 1.5%. Even at a brightness of 5000 cd m^{-2} **GII** showed a CE of 56.8 cd A^{-1} (9.7% roll-off), while **GIII** displayed a CE of 44.8 cd A^{-1} (8.2% roll-off). In contrast a significantly higher overall efficiency roll-off of 55.3% for device **GI**, featuring CE of 28.2 cd $A^{-1}$and 15.7 cd A^{-1} at a brightness of 1000 cd m^{-2} and 5000 cd m^{-2}, was observed. This efficiency roll-off is attributed to the dominant hole transport properties of **o-TPAPOXD**, due to the TPA donor unit (more balanced charge transport for the planarized donor structures; see chapter Charge Transport Properties). The unbalanced charge transport properties lead to accumulation of holes at the interface of the emissive and TPBI layer and a narrow exciton recombination zone. Since triplet-triplet annihilation (TTA) is strongly dependent on the triplet exciton concentration the thickness of the recombination zone is of crucial importance and a major factor for efficiency roll-off in PHOLED devices at high current densities.[51] Thus, the incorporation of planarized arylamine donors significantly decreases the efficiency roll-off as a result of more balanced charge transport properties resulting in broader recombination zones.

Red devices **RI**, **RII** and **RIII** showed similar performance exhibiting CE_{max} of 14.0 cd A^{-1}, 16.1 cd A^{-1} and 15.0 cd A^{-1}, PE_{max} of 13.7 lm W^{-1}, 16.8 lm W^{-1} and 12.2 lm W^{-1} and EQE_{max} of 8.3%, 11.2% and 10.1%. In analogy to the green devices lower

efficiency roll-off was observed for devices **RII** and **RIII** (incorporating planarized host materials) compared to **RI**.

Furthermore, blue device **BII**, utilizing **o-PCzPOXD** as host, was fabricated displaying a CE_{max} of 29.8 cd A^{-1}, a PE_{max} of 33.5 lm W^{-1} and an EQE_{max} of 13.4%. Thus, it was demonstrated that **o-PCzPOXD** is applicable as universal host material in efficient red, green and blue PHOLED devices. However, low device performance has been observed for blue devices applying **o-ICzPOXD**. For these devices also the recorded emission could not be assigned to the FIrPic emitter only. Systematic investigations are necessary to understand these findings.

As a result of the lower triplet energies of the TOXD materials compared to the POXD series, **o-TPATOXD** (**IV**), **o-PCzTOXD** (**V**), **o-ICzTOXD** (**VI**) and **o-CzTOXD** (**VII**) were examined in red (**R**) devices only. Identical device architecture as for the POXD series was applied. Among this series of devices **RIV** exhibited the highest CE_{max} of 28.8 cd A^{-1}, PE_{max} of 28.4 lm W^{-1} and EQE_{max} of 16.9%, while **RV**, **RVI**, **RVII** displayed CE_{max} of 14.4, 19.2 and 12.6 cd A^{-1}, PE_{max} of 10.6, 16.7 and 10.0 lm W^{-1} and EQE_{max} of 11.2%, 13.2% and 9.4%, respectively, displaying similar device performance as the corresponding POXD compounds. The same tendency for decreased efficiency roll-off observed for the POXD series was found for devices **RIV-VII**. While the CE of device **RIV** drops to 10.5 cd A^{-1} at a brightness of 5000 cd m^{-2}, corresponding to an efficiency roll-off of 64%, current efficiencies for devices **RV**, **RVI** and **RVII** (incorporating planarized donors) decreased only by 24% to 27%.

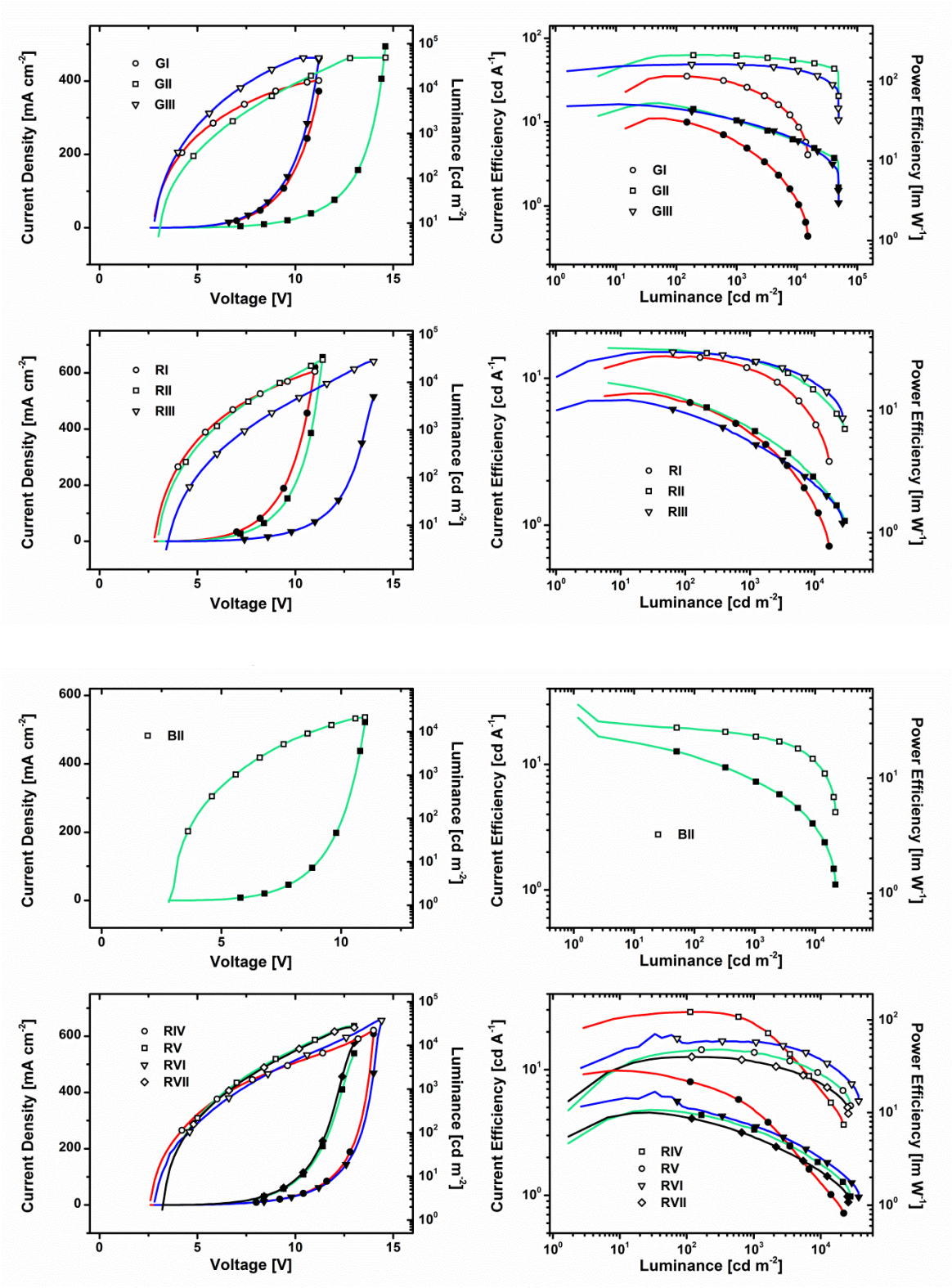

Fig. 7 Current density-voltage-luminance (full symbols: current density, hollow symbols: luminance) and current efficiency-luminance-power efficiency (full symbols: power efficiency, hollow symbols: current efficiency) curves of all devices investigated in this work.

Table 3 Electroluminescent properties of devices **GI-III**, **BII** and **RI-VII**.

	V_{on} [V]	L_{max} [cd m^{-2}]	CE [cd A^{-1}][a]	PE [lm W^{-1}][a]	EQE [%][a]
GI	2.8	15049	35.0/28.2/15.7/35.1	32.3/17.1/6.3/34.4	10.3/8.1/4.7/10.3
GII	3.0	49386	62.3/61.2/56.8/62.9	48.9/31.1/21.5/53.5	17.0/16.4/15.5/17.1
GIII	2.6	48768	48.4/48.1/44.8/48.8	44.9/32.1/22.4/51.6	13.7/13.6/12.7/13.8
BII	2.8	21710	18.9/16.7/13.4/29.8	15.3/9.4/5.6/33.5	8.5/7.5/6.1/13.4
RI	2.8	16838	13.9/11.5/7.4/14.0	11.7/6.4/2.9/13.7	8.2/6.6/4.1/8.3
RII	3.0	29615	15.3/13.2/10.1/16.1	12.4/7.2/4.0/16.8	10.6/9.1/6.7/11.2
RIII	3.0	27517	14.9/12.9/10.8/15.0	9.4/5.3/3.3/12.2	9.1/6.9/5.3/10.1
RIV	2.6	22160	28.7/22.6/10.5/28.8	21.4/10.1/3.0/28.4	16.8/13.2/6.0/16.9
RV	3.2	27768	14.2/13.7/10.9/14.4	9.7/6.5/3.7/10.6	11.1/9.5/7.3/11.2
RVI	2.8	36975	16.2/16.5/14.2/19.2	11.0/7.0/4.3/16.7	11.3/11.4/9.6/13.2
RVII	3.0	25837	12.6/11.4/9.2/12.6	8.6/5.3/3.1/10.0	9.3/7.2/5.8/9.4

[a]Measured at a brightness of 100 cd m^{-2}/1000 cd m^{-2}/5000 cd m^{-2}/max

Conclusion

In this study, the impact of planarizing TAA donors in bipolar host materials on the *ortho*-linkage effect was investigated in detail. Hence, oxadiazole based structures **5a-c** and **8a-d** have been designed, synthesized and examined regarding thermal, photo-physical and electro-chemical properties.

The straight-forward synthesis of target compounds relies on efficient cross-coupling and organolithum based procedures. In particular, the developed C-H activation protocol allows for a convenient and selective access to potential target scaffolds, clearly broadening the scope of accessible indolo[3,2,1-*jk*]carbazole motives.

For increasingly planarized TAA donor structures the following conclusion can be drawn: (i) improved morphological stability; (ii) elevated singlet and triplet energy values, which are attributed to an enhanced *ortho*-linkage effect and reduced donor strength of the planarized structures; (iii) significantly reduced efficiency roll-off for all devices. Hence, the concept of planarization addresses major challenges in PHOLED research: improving both triplet energy and compound stability. In fact, triplet energies of >2.60 eV enable the construction of efficient blue (FIrPic) PHOLEDs, which has not been reported for this specific substance class up to date.

Improved PHOLED performances in standard device configurations compared to non-planarized reference compound **o-TPAPOXD** (EQE_{max} of 22.0% reported for optimized architectures)[17] reveal the great potential for the developed compounds as highly efficient host materials.

Experimental Section

General Information

All reagents and solvents have been purchased from commercial suppliers and used without further purification. Anhydrous solvents were prepared by filtration through drying columns; dry DMF was obtained from Acros. Column chromatography was performed on silica 60 (Merck, 40-63 μm). NMR spectra were recorded on a Bruker Avance DRX-400 Spectrometer or a Bruker Avance 200 Spectrometer. High resolution mass spectra (HRMS) were obtained from a Thermo Scientific LTQ Orbitrap XL hybrid FTMS (Fourier Transform Mass Spectrometer) and Thermo Scientific MALDI LTQ Orbitrap interface; α-cyano-4-hydroxycinnamic acid was used as matrix. Thermogravimetric (TG) and differential scanning calorimetry (DSC) measurements were carried out with a heating rate of 5 K/min in a flowing argon atmosphere (25 mL/min). For the TG measurements, a Netsch TG 209 F9 Tarsus system, working with open aluminium oxide crucibles, was used. For the DSC measurements, a Netsch DSC 200 F3 Maia, working with aluminium pans with pierced lids, was employed. UV/VIS absorption and fluorescence emission spectra were recorded in DCM solutions (5 μM) with a Perkin Elmer Lambda *750* spectrometer and an Edinburgh FLS920, respectively. Time resolved experiments were obtained using a Quantel Brilliant tripled Nd-YAG laser (355 nm, 20 Hz repetition rate, pulse width ~5 ns). Spectra were measured using a SPEX 270 monochromator equipped with both photomultiplier and CCD. This set-up is controlled using a home-built Labview-based program which allows using different instruments such as photon counting, oscilloscope, and additional mechanical shutters. For the measurement of the triplet emission, a mechanical shutter was triggered by the pulsed laser. A pretrigger period of 0.5 ms was followed by a 1 ms

aperture and a rest time of 300 – 500 ms allowed obtaining the measurements shown in the ESI. The slit of the monochromator was also opened further (up to 0.5 mm) to measure the triplet emission. Triplet energy (E_T) values were determined form the highest energy vibronic subband (first significant peak/shoulder) of the time-resolved low-temperature phosphorescence spectra. Cyclic voltammetry was performed using a three electrode configuration consisting of a Pt working electrode, a Pt counter electrode and an Ag/AgCl reference electrode and a PGSTAT128N, ADC164, DAC164, External, DI048 potentiostat provided by Metrohm Autolab B.V. Measurements were carried out in a 0.5 mM solution in anhydrous DCM (oxidation scan) and THF or DMF (reduction scan) with Bu_4NBF_4 (0.1 M) as supporting electrolyte. The solutions were purged with nitrogen for 15 minutes prior to measurement. HOMO and LUMO energy levels were calculated from the onset of oxidation and reduction, respectively. The onset potential was determined by the intersection of two tangents drawn at the background and the rising of oxidation or reduction peaks.

Synthetic Details

N,*N*-Diphenyl-4-(4,4,5,5-tetramethyl-1,3,2-dioxaborolan-2-yl)benzeneamine (**3a**),[18,19] 9-[4-(4,4,5,5-tetramethyl-1,3,2-dioxaborolan-2-yl)phenyl]-9*H*-carbazole (**3b**),[19,20] 2,5-bis(5-bromo-2-thienyl)-1,3,4-oxadiazole (**4**),[52] and 2,5-bis(2-bromophenyl)-1,3,4-oxadiazole (**6**)[27] have been prepared according to published procedures.

9-(2-Chlorophenyl)-9*H*-carbazole (1ii). 1ii was synthesized following procedures in literature.[20] Carbazole (2.51 g, 15.0 mmol, 1.00 eq.), 1-bromo-2-chlorobenzene (3.45 g, 18.0 mmol, 1.20 eq.), K_2CO_3 (2.07 g, 15.0 mmol, 1.00 eq.) and $CuSO_4 \cdot 5H_2O$ (0.19 g, 0.75 mmol, 0.05 eq) were added to a 250 ml three-necked round-bottomed flask.

The mixture was heated with a heating jacket to 230 °C for 72 h. After cooling to r.t. H_2O (100 ml) was added and the mixture was extracted with toluene. The brown suspension was filtrated and the remaining solvent removed in *vacuo*. Purification by crystallization from EtOH yielded **1ii** as white solid (1.93 g, 6.9 mmol, 46%). ^{1}H NMR (400 MHz, $CDCl_3$): δ = 8.21 (d, J=7.7 Hz, 2H), 7.73-7.71 (m, 1H), 7.56-7.44 (m, 5H), 7.35 (t, J=7.5 Hz, 2H), 7.15 (d, J=8.1 Hz, 2H) ppm. ^{13}C NMR (100 MHz, $CDCl_3$): δ = 140.8 (s), 135.0 (s), 133.7 (s), 131.0 (d), 130.8 (d), 129.8 (d), 128.1 (d), 125.9 (d), 123.3 (s), 120.3 (d), 120.0 (d), 109.9 (d) ppm. Calculated: *m/z* 277.07 $[M]^+$. Found: MS (EI): *m/z* 277.03 $[M]^+$.

2,6-Dichloro-*N*,*N*-diphenylbenzenamine (1iii). Diphenylamine (1.02 g, 6.0 mmol, 1.00 eq.) was dissolved in dry DMF (18 ml). The solution was purged with argon, subsequently heated to 50 °C and NaH (0.43 g, 18.0 mmol, 3.00 eq.) was added quickly. The suspension was stirred for 5 min at 50 °C before 1,3-dichloro-2-fluorobenzene (1.49, 9.0 mmol, 1.50 eq.) was added. Due to incomplete conversion (TLC) after stirring overnight additional NaH (0.14 g, 6.0 mmol 1.00 eq.) was added. After full conversion (TLC – 24 h) the reaction mixture was poured on H_2O, extracted with DCM repeatedly and the combined organic layers were dried over Na_2SO_4 and concentrated under reduced pressure. Column chromatography (PE) yielded **1iii** (0.79 g, 2.5 mmol, 42%) as white solid. ^{1}H NMR (400 MHz, CD_2Cl_2): δ = 7.46 (d, J=8.1 Hz, 2H), 7.29-7.22 (m, 5H), 6.99-7.96 (m, 6H) ppm. ^{13}C NMR (100 MHz, CD_2Cl_2): δ = 145.7 (s), 140.7 (s), 137.6 (s), 130.2 (d), 129.6 (d), 129.3 (d), 122.6 (d), 121.0 (d) ppm. Calculated: *m/z* 313.04 $[M]^+$. Found: MS (EI): *m/z* 313.01 $[M]^+$.

Indolo[3,2,1-*jk*]carbazole (2). 1i/1ii/1iii (1.0 eq.), (NHC)Pd(allyl)Cl[24,25] (2 mol%) and K_2CO_3 (2.00 eq.) were dissolved in degassed *N*,*N*-dimethylacetamide (DMA, 0.2 M) under argon atmosphere and heated to 130 °C until complete conversion (GCMS).

The reaction mixture was poured on water and extracted with Et_2O. The combined organic layers were dried over anhydrous Na_2SO_4 and the solvent was removed under reduced pressure. Purification was accomplished by column chromatography (PE). Starting from **1i** (9.66 g, 30.0 mmol), (NHC)Pd(allyl)Cl (0.34 g, 0.60 mmol) and K_2CO_3 (8.29 g, 60.0 mmol) **2** was obtained as white powder (6.78 g, 28.1 mmol, 94%). Starting from **1ii** (3.70 g, 13.3 mmol), (NHC)Pd(allyl)Cl (0.15 g, 0.27 mmol) and K_2CO_3 (3.67 g, 26.6 mmol) **2** was obtained as white powder (3.02 g, 12.5 mmol 94%). Starting from **1iii** (0.47 g, 1.5 mmol), (NHC)Pd(allyl)Cl (0.02 g, 0.03 mmol) and K_2CO_3 (0.43 g, 3.1 mmol) **2** was obtained as white powder (0.29 g, 1.2 mmol, 80%). ^{1}H NMR (400 MHz, CD_2Cl_2): δ = 8.16 (d, J=7.8 Hz, 2H), 8.06 (d, J=7.4 Hz, 2H), 7.92 (d, J=8.1 Hz, 2H), 7.62-7.55 (m, 3H), 7.38 (t, J=7.7 Hz, 2H) ppm. ^{13}C NMR (100 MHz, CD_2Cl_2): δ = 144.2 (s), 139.2 (s), 130.5 (s), 127.3 (d), 123.6 (d), 123.4 (d), 122.3 (d), 119.9 (d), 118.9 (s), 112.7 (d) ppm. Calculated: *m/z* 241.09 $[M]^+$. Found: MS (EI): *m/z* 241.11 $[M]^+$.

2-Bromoindolo[3,2,1-*jk*]carbazole. 2 (14.26 g, 59.1 mmol, 1.0 eq.) was dissolved in AcOH / $CHCl_3$ = 1:1 (300 ml) and heated to 55 °C. NBS (10.51 g, 59.1 mmol, 1.0 eq.) was added in small portions over a period of 1 h to the grey suspension. Since GC-MS analysis indicated incomplete conversion, more NBS (1.05 g, 5.9 mmol, 0.10 eq.) was added. After complete conversion the reaction was poured on aqueous NaOH solution (1000 ml, 6M, 2 eq.) and extracted with DCM. The organic layer was dried over Na_2SO_4 and the solvent was removed *in vacuo*. Crystallization from ACN yielded 2-bromoindolo[3,2,1-*jk*]carbazole as beige powder (10.30 g, 32.2 mmol, 54%). Physical data in accordance to literature.[23]

2-(4,4,5,5-Tetramethyl-1,3,2-dioxaborolan-2-yl)indolo[3,2,1-*jk*]carbazole (3c). The synthesis of **3c** was accomplished analogously to published procedures.[19,23] To

a solution of 2-bromoindolo[3,2,1-*jk*]carbazole (10.25 g, 32.0 mmol, 1.00 eq.) in anhydrous THF (100 mL) under argon atmosphere *n*-BuLi (14.1 ml, 2.5 M in hexanes, 35.2 mmol, 1.10 eq.) was added dropwise at -78 °C. Subsequently the reaction mixture was stirred at -80 °C for 1 h before Pinbop® (7.14 g, 38.4 mmol, 1.20 eq.) was added and the reaction was allowed to warm to room temperature slowly. After stirring overnight the solvent was removed under reduced pressure and the residue was partitioned between aqueous HCl (1N) and DCM. The aqueous phase was extracted with DCM, the combined organic layers were dried over anhydrous Na_2SO_4 and concentrated *in vacuo*. **3c** (8.10 g, 22.1 mmol, 69%) was isolated as white solid after crystallization from acetonitrile. ^{1}H NMR (400 MHz, $CDCl_3$): δ = 8.58 (s, 2H), 8.14 (d, J=7.7 Hz, 2H), 7.90 (d, J=8.0 Hz, 2H), 7.56 (dd, J=8.0, 7.6 Hz, 2H), 7.37 (dd, J=7.7, 7.6 Hz, 2H), 1.46 (s, 12H) ppm. ^{13}C NMR (100 MHz, $CDCl_3$): δ = 145.9 (s), 138.9 (s), 130.0 (s), 126.7 (d), 126.3 (d), 123.2 (d), 122.0 (d), 118.2 (s), 112.2 (d), 83.8 (s), 25.0 (s) ppm (C–B not detected). Calculated: *m/z* 367.17381 $[M]^+$, 368.18164 $[M+H]^+$. Found: MS (MALDI): *m/z* 367.17526 $[M]^+$, 368.17856 $[M+H]^+$.

General procedure for the Suzuki cross coupling towards 5a-c. The reactions towards **5a**-**c** were performed under argon atmosphere. **4** (1.00 eq.) and boronic acid ester **3a**-**c** (2.50 eq.) were dissolved in degassed THF (~0.5 M). Subsequently degassed 2 M aqueous K_2CO_3 (5.00 eq.) and $Pd(PPh_3)_4$ (5 mol%) were added. The reaction mixture was heated to reflux until full conversion of the dibromide (4-20 h, TLC). Afterwards the solution was poured on water and repeatedly extracted with DCM. The combined organic layers were dried over anhydrous Na_2SO_4 and concentrated under reduced pressure. The crude products were purified by column chromatography.

2',2''-(1,3,4-Oxadiazole-2,5-diyl)bis[*N*,*N*-diphenyl[1,1'-biphenyl]-4-amine] (5a). Starting from **4** (0.27 g, 0.70 mmol), **3a** (0.65 g, 1.75 mmol), 1.75 ml aqueous K_2CO_3 solution and $Pd(PPh_3)_4$ (40 mg, 35 µmol) **5a** (0.42 g, 0.59 mmol, 85%) was isolated after column chromatography (DCM) as white solid. Physical data according to literature.[16]

9,9'-(1,3,4-Oxadiazole-2,5-diyldi(1,1'-biphenyl)-2',4-diyl)bis[9*H*-carbazole] (5b). Starting from **4** (0.19 g, 0.50 mmol), **3b** (0.46 g, 1.25 mmol), 1.25 ml aqueous K_2CO_3 solution (2.5 mmol) and $Pd(PPh_3)_4$ (29 mg, 25 µmol) **5b** (0.33 g, 93%) was isolated after column chromatography (DCM) as white solid. ^{1}H NMR (400 MHz, CD_2Cl_2): δ = 8.14 (d, J=7.7 Hz, 4H), 7.96 (d, J=7.8 Hz, 2H), 7.69 (ddd, J=7.6, 7.5, 1.1 Hz, 2H), 7.56-7.49 (m, 8H), 7.40-7.21 (m, 16H) ppm. ^{13}C NMR (100 MHz, CD_2Cl_2): δ = 165.6 (s), 141.6 (s), 141.3 (s), 140.1 (s), 137.4 (s), 132.1 (d), 131.7 (d), 131.0 (d), 130.6 (d), 128.7 (d), 127.2 (d), 126.6 (d), 123.9 (s), 123.3 (s), 120.8 (d), 120.5 (d), 110.1 (d) ppm. Calculated: m/z 704.25706 $[M]^+$, 705.26489 $[M+H]^+$, 727.24683 $[M+Na]^+$. Found: MS (MALDI): m/z 704.25807 $[M]^+$, 705.26586 $[M+H]^+$, 727.24966 $[M+Na]^+$.

2,2'-(1,3,4-Oxadiazole-2,5-diyldi-2,1-phenylene)bis[indolo[3,2,1-*jk*]carbazole] (5c). Starting from **4** (0.76 g, 2.0 mmol), **3c** (1.84 g, 5.0 mmol), 5 ml aqueous K_2CO_3 solution (10 mmol) and $Pd(PPh_3)_4$ (0.12 g, 0.1 mmol) **5c** (0.55 g, 0.8 mmol, 39%) was isolated after column chromatography (DCM) as white solid. ^{1}H NMR (400 MHz, CD_2Cl_2): δ = 8.09 (d, J=7.8 Hz, 4H), 7.98 (d, J=8.1 Hz, 4H), 7.91 (s, 4H), 7.61 (dd, J=7.7, 7.7 Hz, 4H), 7.50-7.30 (m, 10 H), 7.01 (dd, J=7.7, 7.7 Hz, 2H) ppm. ^{13}C NMR (100 MHz, CD_2Cl_2): δ = 165.0 (s), 144.0 (s), 143.9 (s), 139.7 (s), 136.8 (s), 132.6 (d), 131.3 (d), 130.4 (s), 129.8 (d), 127.7 (d), 127.6 (d), 123.8 (d), 123.7 (s), 122.4 (d), 121.2 (d), 118.5 (s), 112.9 (d) ppm. Calculated: m/z 700.22576 $[M]^+$, 701.23359

$[M+H]^+$, 723.21553 $[M+Na]^+$. Found: MS (MALDI): m/z 700.22461 $[M]^+$, 701.23624 $[M+H]^+$, 723.21879 $[M+Na]^+$.

General procedure for double-sided Halogen Dance reactions. A protocol described in literature[53] was adopted for the double-sided Halogen Dance reaction. Freshly prepared LDA was used. To a solution of diisopropylamine (2.40 eq.) in anhydrous THF (0.75 M), *n*-BuLi (2.40 eq., 2.5 M in hexanes) was slowly added at 0 – 5 °C and the solution was stirred for 30 min. Subsequently, the LDA solution was added dropwise to dibromide **6** (1.00 eq.) dissolved in anhydrous THF (25 mM) at -25 °C *via* a syringe. The temperature was remained at -25 °C for 30 min before the reaction was quenched with an electrophile and warmed to room temperature. For work up the THF was removed under reduced pressure, the remaining oil was dissolved in DCM and washed with water. The aqueous phase was extracted with DCM, the combined organic layers were dried over anhydrous Na_2SO_4 and the solvent was removed *in vacuo*. Purification was accomplished by column chromatography.

2,5-Bis(3-bromo-2-thienyl)-1,3,4-oxadiazole (7i). Starting from DIPA (0.18 g, 1.8 mmol), *n*-BuLi (0.72 ml, 1.8 mmol), **6** (0.29 g, 0.75 mmol) and MeOH (0.25 ml) **7i** (0.16 g, 0.40 mmol, 53%) was yielded after column chromatography (light petrol:Et_2O = 60:40) as white solid. ^{1}H NMR (400 MHz, $CDCl_3$): δ = 7.52 (d, J=5.3 Hz, 2H), 7.16 (d, J=5.3 Hz, 2H) ppm. ^{13}C NMR (100 MHz, $CDCl_3$): δ = 159.2 (s), 132.8 (d), 130.2 (d), 120.9 (s), 114.0 (s) ppm. Calculated: *m/z* 390.82046 $[M+H]^+$, 412.80240 $[M+Na]^+$. Found: MS (MALDI): *m/z* 390.82188 $[M+H]^+$, 412.80376 $[M+Na]^+$.

2,5-Bis(3-bromo-5-trimethylsilyl-2-thienyl)-1,3,4-oxadiazole (7ii). Starting from DIPA (0.18 g, 1.80 mmol), *n*-BuLi (0.72 ml, 1.80 mmol), **6** (0.29 g, 0.75 mmol) and TMSBr (0.35 g, 2.25 mmol, 3.00 eq.) **7ii** (0.17 mg, 0.31 mmol, 42%) was yielded after

column chromatography (light petrol:Et_2O = 95:5) as colorless oil, that solidified after an extended period of time at -30 °C. ^{1}H NMR (400 MHz, $CDCl_3$): δ = 7.22 (s, 2H), 0.37 (s, 18H) ppm. ^{13}C NMR (100 MHz, $CDCl_3$): δ = 159.2 (s), 147.0 (s), 138.6 (d), 125.0 (s), 114.6 (s), -0.5 (q) ppm. Calculated: *m/z* 534.89951 $[M+H]^+$, 556.88145 $[M+Na]^+$. Found: MS (MALDI): *m/z* 534.90132 $[M+H]^+$, 556.88296 $[M+Na]^+$.

General procedure for the Suzuki cross coupling reaction of 7i and boronic acid esters 3a-c. Target compounds **8a**-**c** were synthesized by a Suzuki cross-coupling procedure according to a published protocol.[24] Dibromide **7i** (1.00 eq.), boronic acid esters **3a**-**c** (3.00 eq.), KO^{t}Bu (3.00 eq.) and (NHC)Pd(allyl)Cl[24,25] (2 mol%) were suspended in ^{i}PrOH/H_2O (3/1, 5 mM) under argon atmosphere. The mixture was heated to reflux until full conversion (4-20 h, TLC), poured on H_2O and repeatedly extracted with DCM. The combined organic layers were dried over anhydrous Na_2SO_4 and the solvent removed in *vacuo*.

4,4'-(1,3,4-Oxadiazole-2,5-diyldi-2,3-thiophenediyl)bis[*N*,*N*-diphenylbenzenamine] (8a). Starting from **7i** (1.76 g, 4.5 mmol), **3a** (5.01 g, 13.5 mmol), KO^{t}Bu (1.51 g, 13.5 mmol) and (NHC)Pd(allyl)Cl (51 mg, 90 µmol) **8a** (1.97 g, 2.7 mmol, 61%) was isolated after column chromatography (light petrol:DCM = 35:65 -> 0:100) as yellow solid. ^{1}H NMR (400 MHz, CD_2Cl_2): δ = 7.56 (d, J=5.1 Hz, 2H), 7.31-7.24 (m, 12H), 7.19 (d, J=5.1 Hz, 2H), 7.12-7.03 (m, 12H), 6.98 (d, J=8.5 Hz, 4H) ppm. ^{13}C NMR (100 MHz, CD_2Cl_2): δ = 160.9 (s), 148.4 (s), 148.0 (s), 145.4 (s), 131.8 (d), 130.6 (d), 129.9 (d), 129.6 (d), 128.8 (s), 125.4 (d), 123.9 (d), 122.9 (d), 118.9 (s) ppm. Calculated: m/z 720.20120 $[M]^+$, 721.20903 $[M+H]^+$, 743.19097 $[M+Na]^+$. Found: MS (MALDI): m/z 720.20177 $[M]^+$, 721.20580 $[M+H]^+$, 743.19167 $[M+Na]^+$.

9,9'-[1,3,4-Oxadiazole-2,5-diylbis(2,3-thiophenediyl-4,1-phenylene)]bis[9*H*-carbazole] (8b). Starting from **7i** (78 mg, 0.20 mmol), **3b** (222 mg, 0.60 mmol), KO^{t}Bu (67 mg, 0.60 mmol) and (NHC)Pd(allyl)Cl (2.3 mg, 4 µmol) **8b** (78 mg, 0.11 mmol, 55%) was isolated after column chromatography (light petrol:DCM = 80:20) as white solid. ^{1}H NMR (400 MHz, CD_2Cl_2): δ = 8.16 (d, J=7.7 Hz, 4H), 7.74 (d, J=8.4 Hz, 4 H), 7.64-7.62 (m, 6H), 7.49 (d, J=8.1 Hz, 4H), 7.40 (ddd, J=8.2, 7.3, 1.2 Hz, 4H), 7.32-7.28 (m, 6H) ppm. ^{13}C NMR (100 MHz, CD_2Cl_2): δ = 160.8 (s), 144.9 (s), 141.2 (s), 138.1 (s), 134.4 (s), 131.9 (d), 131.3 (d) 130.1 (d), 127.1 (d), 126.5 (d), 124.0 (s), 120.8 (d), 120.6 (d), 120.1 (s), 110.4 (d) ppm. Calculated: m/z 716.16990 $[M]^+$, 717.17773 $[M+H]^+$, 739.15967 $[M+Na]^+$. Found: MS (MALDI): m/z 716.17188 $[M]^+$, 717.17841 $[M+H]^+$, 739.16278 $[M+Na]^+$.

2,2'-(1,3,4-Oxadiazole-2,5-diyldi-2,3-thiophenediyl)bis[indolo[3,2,1-*jk*]carbazole] (8c). Starting from **7i** (118 mg, 0.30 mmol), **3c** (330 mg, 0.90 mmol), KO^{t}Bu (101 mg, 0.90 mmol) and (NHC)Pd(allyl)Cl (3.4 mg, 6 µmol) **8c** (158 mg, 0.22 mmol, 74%) was isolated after column chromatography (DCM) as white solid. ^{1}H NMR (400 MHz, d_6-DMSO): δ = 8.03-8.00 (m, 8H), 7.93-7.87 (m, 6H), 7.57 (dd, J=7.7, 7.7 Hz, 4H), 7.38-7.34 (m, 6H) ppm. ^{13}C NMR (100 MHz, d_6-DMSO): δ = 159.9, 146.1, 142.5, 138.1, 132.5, 130.4, 129.2, 129.0, 127.1. 123.2, 121.9, 120.9, 117.8, 117.1, 112.7 ppm. Calculated: m/z 712.13860 $[M]^+$, 713.14643 $[M+H]^+$, 735.12837 $[M+Na]^+$. Found: MS (MALDI): m/z 712.13611 $[M]^+$, 713.14685 $[M+H]^+$, 735.129520 $[M+Na]^+$.

9,9'-(1,3,4-Oxadiazole-2,5-diyldi-2,3-thiophenediyl)bis[9*H*-carbazole] (8d). **7i** (2.16 g, 5.5 mmol, 1.0 eq.), carbazole (2.76 g, 16.5 mmol, 3.0 eq.) K_2CO_3 (2.28 g, 16.5 mmol, 3.0 eq.) and $CuSO_4 \cdot 5H_2O$ (88 mg, 0.35 mmol, 6.4 mol%) were mixed in a sealed reaction vial and heated to 230 °C. After cooling the reaction mixture was dissolved in $CHCl_3$, washed with water and the aqueous phase was extracted with

$CHCl_3$. The combined organic layers were dried over anhydrous Na_2SO_4 and concentrated under reduced pressure. **8d** (0.81 g, 1.4 mmol, 26%) was isolated after column chromatography (light petrol:DCM = 85:15 -> 78:22) as white solid. ^{1}H NMR (400 MHz, CD_2Cl_2): δ = 8.13 (d, J=7.7 Hz, 4H), 7.67 (d, J=5.3 Hz, 2H), 7.36-7.23 (m, 10H), 7.04 (d, J=7.9 Hz, 4H) ppm. ^{13}C NMR (100 MHz, CD_2Cl_2): δ = 158.6 (s), 141.2 (s), 137.2 (s), 130.7 (d), 128.7 (d), 128.6 (d), 124.1 (s), 120.9 (d), 120.9 (d), 119.9 (s), 110.5 (d) ppm. Calculated: m/z 564.10730 $[M]^+$, 565.11513 $[M+H]^+$, 587.09707 $[M+Na]^+$. Found: MS (MALDI): m/z 564.10961 $[M]^+$, 565.11649 $[M+H]^+$, 587.09908 $[M+Na]^+$.

Computational Details

All computations were performed using the Gaussian 09 package, revision A.02.[54] Density functional theory (DFT) and time-dependent (TD) DFT calculations were performed using the Becke three parameters hybrid functional with Lee–Yang–Perdew correlation (B3LYP),[55,56] in combination with Pople basis sets (6-31G*, 6-311+G*).[57] Geometry optimizations were performed in gas phase and without symmetry constraints. For the calculation of HOMO/LUMO levels, ground state (S_0) geometries were optimized applying the 6-311+G* basis set. The determination of triplet energy (E_T) was achieved by the calculation of the T_1 excitation energy applying TDDFT level and the 6-311+G* basis to a S_0 geometry optimized at DFT level using the 6-31G* basis set.

Single crystal diffraction

Single crystals were obtained by recrystallization from hot solvents (**3c** – acetonitrile, **5b** – toluene, **8b** – toluene). Crystals of **3c**, **o-PCzPOXD** (**5b**) and **o-PCzTOXD** (**8b**) suitable for single-crystal diffraction were selected under a polarizing microscope, embedded in perfluorinated oil and attached to Kapton® micro-mounts. Intensity data were collected on a Bruker KAPPA APEX II diffractometer equipped with a CCD detector using MoKα radiation (λ = 0.71072 Å). Data were reduced with SAINT-Plus[58] and an absorption correction was applied using the multi-scan approach implemented in SADABS.[58] All non-H atoms were located in the electron-density maps obtained by charge-flipping implemented in SUPERFLIP.[59] The structures were refined against *F* values using JANA2006.[60] H atoms were placed at computed positions and refined as riding on the parent C atoms. All non-H atoms were refined with anisotropic displacement parameters.

Device Fabrication and Measurement

The devices were fabricated on cleaned glass substrates pre-coated by a 180 nm thickness of indium-tin-oxide (ITO) with a sheet resistance of 10 Ω per square. Prior to deposition, the surface of ITO was treated by oxygen plasma for 2 min, following a degrease in an ultrasonic solvent bath. All layers were deposited by thermal evaporation in a high vacuum system (pressure $<10^{-4}$ Pa) without breaking the vacuum. The device structures were described in the text. For the case of doping, the deposition rates of both host and guest were measured by a quartz crystal oscillators, and monitored by a frequency counter and calibrated by a Dektak 6M profiler (Veeco). The aluminum (Al) electrodes were deposited on the organic films through

shadow masks. The overlap between ITO and Al electrode was 4 mm × 4 mm as the active emissive area of the devices.

The current-voltage-brightness characteristics were measured by using a Keithley source measurement unit (Keithley 2400 and Keithley 2000) with a calibrated silicon photodiode. The electroluminescence (EL) spectra were measured by a Spectrascan PR650 spectrophotometer. All the measurements were carried out in ambient atmosphere at room temperature.

Acknowledgement

This work was supported in part by the Swiss National Science Foundation. The authors thank F.-A. Miannay and B. Lang (University of Geneva) for help with the picoseconds lifetime measurements. The X-ray centre of the Vienna University of Technology is acknowledged for providing access to the single-crystal diffractometer. G. Fafilek is acknowledged for support regarding the CV measurements, B. Holzer for collaboration during the synthetic experiments, K. Föttinger assisting the photo-physical analysis and J. Chen for fruitful discussions.

References

1. C. W. Tang and S. A. VanSlyke, *Appl. Phys. Lett.*, 1987, **51**, 913-915.
2. S. R. Forrest, *Nature*, 2004, **428**, 911-918.
3. Y. Sun, N. C. Giebink, H. Kanno, B. Ma, M. E. Thompson and S. R. Forrest, *Nature*, 2006, **440**, 908-912.
4. S. Reineke, F. Lindner, G. Schwartz, N. Seidler, K. Walzer, B. Luessem and K. Leo, *Nature*, 2009, **459**, 234-238.
5. M. C. Gather, A. Koehnen and K. Meerholz, *Adv. Mater.*, 2011, **23**, 233-248.
6. L. Xiao, Z. Chen, B. Qu, J. Luo, S. Kong, Q. Gong and J. Kido, *Adv. Mater.*, 2011, **23**, 926-952.
7. Y. Tao, C. Yang and J. Qin, *Chem. Soc. Rev.*, 2011, **40**, 2943-2970.
8. M. A. Baldo, D. F. O'Brien, Y. You, A. Shoustikov, S. Sibley, M. E. Thompson and S. R. Forrest, *Nature*, 1998, **395**, 151-154.
9. M. A. Baldo, S. Lamansky, P. E. Burrows, M. E. Thompson and S. R. Forrest, *Appl. Phys. Lett.*, 1999, **75**, 4-6.
10. P.-T. Chou and Y. Chi, *Chem. - Eur. J.*, 2007, **13**, 380-395.
11. Y. Chi and P.-T. Chou, *Chem. Soc. Rev.*, 2010, **39**, 638-655.
12. M. A. Baldo, D. F. O'Brien, M. E. Thompson and S. R. Forrest, *Phys. Rev. B: Condens. Matter Mater. Phys.*, 1999, **60**, 14422-14428.
13. C. Adachi, M. A. Baldo, M. E. Thompson and S. R. Forrest, *J. Appl. Phys.*, 2001, **90**, 5048-5051.
14. M. A. Baldo, C. Adachi and S. R. Forrest, *Phys. Rev. B: Condens. Matter Mater. Phys.*, 2000, **62**, 10967-10977.
15. Y. Tao, Q. Wang, C. Yang, Q. Wang, Z. Zhang, T. Zou, J. Qin and D. Ma, *Angew. Chem., Int. Ed.*, 2008, **47**, 8104-8107.
16. Y. Tao, Q. Wang, Y. Shang, C. Yang, L. Ao, J. Qin, D. Ma and Z. Shuai, *Chem. Commun.*, 2009, 77-79.
17. Y. Tao, Q. Wang, C. Yang, J. Qin and D. Ma, *ACS Appl. Mater. Interfaces*, 2010, **2**, 2813-2818.
18. H. B. Goodbrand and N.-X. Hu, *J. Org. Chem.*, 1999, **64**, 670-674.
19. R. Anemian, D. C. Cupertino, P. R. Mackie and S. G. Yeates, *Tetrahedron Lett.*, 2005, **46**, 6717-6721.
20. H. Xu, K. Yin and W. Huang, *Chem. - Eur. J.*, 2007, **13**, 10281-10293.
21. J. Lv, Q. Liu, J. Tang, F. Perdih and K. Kranjc, *Tetrahedron Lett.*, 2012, **53**, 5248-5252.
22. H. G. Dunlop and S. H. Tucker, *J. Chem. Soc.*, 1939, 1945-1956.
23. S. I. Wharton, J. B. Henry, H. McNab and A. R. Mount, *Chem. - Eur. J.*, 2009, **15**, 5482-5490.
24. N. Marion, O. Navarro, J. Mei, E. D. Stevens, N. M. Scott and S. P. Nolan, *J. Am. Chem. Soc.*, 2006, **128**, 4101-4111.
25. O. Navarro and S. P. Nolan, *Synthesis*, 2006, 366-367.
26. (**3c**): $C_{24}H_{22}BNO_2$, M_r = 367.3, trigonal, $R\,\bar{3}$, $a = b$ = 30.3853(6) Å, c = 10.5350(2) Å, V = 8423.5(3) Å^3, Z = 18, μ = 0.081 mm^{-1}, T = 100 K, 124 955 measured, 11 591 independent and 9 475 observed [$I > 3\sigma(I)$] reflections, 253 parameters, wR (all data) = 0.060, R [$I > 3\sigma(I)$] = 0.041; CCDC reference number 955416.
27. X. Zheng, Z. Li, Y. Wang, W. Chen, Q. Huang, C. Liu and G. Song, *J. Fluorine Chem.*, 2003, **123**, 163-169.
28. S. Zrig, G. Koeckelberghs, T. Verbiest, B. Andrioletti, E. Rose, A. Persoons, I. Asselberghs and K. Clays, *J. Org. Chem.*, 2007, **72**, 5855-5858.
29. J. Froehlich, *Prog. Heterocycl. Chem.*, 1994, **6**, 1-35.
30. M. Schnuerch, M. Spina, A. F. Khan, M. D. Mihovilovic and P. Stanetty, *Chem. Soc. Rev.*, 2007, **36**, 1046-1057.
31. d. S. M. V. Nora, *Curr. Org. Chem.*, 2007, **11**, 637-646.
32. A. E. Lozano, M. L. Jimeno, J. de Abajo and J. G. de la Campa, *Macromolecules*, 1994, **27**, 7164-7170.
33. N. Miyaura, K. Yamada and A. Suzuki, *Tetrahedron Lett.*, 1979, 3437-3440.
34. N. Miyaura and A. Suzuki, *J. Chem. Soc., Chem. Commun.*, 1979, 866-867.
35. N. Miyaura and A. Suzuki, *Chem. Rev. (Washington, D. C.)*, 1995, **95**, 2457-2483; and references cited therein.
36. F. Ullmann, *Ber. Dtsch. Chem. Ges.*, 1903, **36**, 2382-2384.
37. F. Ullmann, *Ber. Dtsch. Chem. Ges.*, 1904, **37**, 853-854.
38. S. V. Ley and A. W. Thomas, *Angew. Chem., Int. Ed.*, 2003, **42**, 5400-5449; and references cited therein.
39. Z. Ge, T. Hayakawa, S. Ando, M. Ueda, T. Akiike, H. Miyamoto, T. Kajita and M.-a. Kakimoto, *Adv. Funct. Mater.*, 2008, **18**, 584-590.

40. Z. Ge, T. Hayakawa, S. Ando, M. Ueda, T. Akiike, H. Miyamoto, T. Kajita and M.-a. Kakimoto, *Org. Lett.*, 2008, **10**, 421-424.
41. Y. Tao, Q. Wang, C. Yang, C. Zhong, K. Zhang, J. Qin and D. Ma, *Adv. Funct. Mater.*, 2010, **20**, 304-311.
42. J. F. Ambrose and R. F. Nelson, *J. Electrochem. Soc.*, 1968, **115**, 1159-1164.
43. J. F. Ambrose, L. L. Carpenter and R. F. Nelson, *J. Electrochem. Soc.*, 1975, **122**, 876-894.
44. (**5b**): $C_{50}H_{32}N_4O$, M_r = 704.8, orthorhombic, $Pna2_1$, a = 17.9874(4) Å, b = 9.2989(8) Å, c = 21.5822(9) Å, V = 3609.9(4) Å^3, Z = 4, μ = 0.078 mm^{-1}, T = 100 K, 146 762 measured, 3 589 independent and 10 547 observed [$I > 3\sigma(I)$] reflections, 496 parameters, wR (all data) = 0.044, R [$I > 3\sigma(I)$] = 0.040; CCDC reference number 955417.
45. (**8b**): $C_{46}H_{28}N_4OS_2$, M_r = 716.9, orthorhombic, $Pna2_1$, a = 16.6992(7) Å, b = 8.3716(3) Å, c = 49.404(2) Å, V = 6906.7(5) Å^3, Z = 8, μ = 0.199 mm^{-1}, T = 100 K, 124 623 measured, 15 888 independent and 12 302 observed [$I > 3\sigma(I)$] reflections, 955 parameters, wR (all data) = 0.036, R [$I > 3\sigma(I)$] = 0.036; CCDC reference number 955418.
46. B. Stoeger, P. Kautny, D. Lumpi, E. Zobetz and J. Froehlich, *Acta Crystallogr B*, 2012, **68**, 667-676.
47. M. Ikai, S. Tokito, Y. Sakamoto, T. Suzuki and Y. Taga, *Appl. Phys. Lett.*, 2001, **79**, 156-158.
48. D.-H. Lee, Y.-P. Liu, K.-H. Lee, H. Chae and S. M. Cho, *Org. Electron.*, 2010, **11**, 427-433.
49. M. E. Kondakova, T. D. Pawlik, R. H. Young, D. J. Giesen, D. Y. Kondakov, C. T. Brown, J. C. Deaton, J. R. Lenhard and K. P. Klubek, *J. Appl. Phys.*, 2008, **104**, 094501-1-094501-7.
50. S. H. Kim, J. Jang, K. S. Yook, J. Y. Lee, M.-S. Gong, S. Ryu, G.-k. Chang and H. J. Chang, *J. Appl. Phys.*, 2008, **103**, 054502-1-054502-4.
51. Q. Fu, J. Chen, H. Zhang, C. Shi and D. Ma, *Opt. Express*, 2013, **21**, 11078-11085.
52. L. G. Liu, Y. F. Xu, X. H. Qian and Q. C. Huang, *Chin. Chem. Lett.*, 2004, **15**, 7-10.
53. J. Froehlich, C. Hametner and W. Kalt, *Monatsh. Chem.*, 1996, **127**, 325-330.
54. M. J. Frisch, G. W. Trucks, H. B. Schlegel, G. E. Scuseria, M. A. Robb, J. R. Cheeseman, G. Scalmani, V. Barone, B. Mennucci, G. A. Petersson, H. Nakatsuji, M. Caricato, X. Li, H. P. Hratchian, A. F. Izmaylov, J. Bloino, G. Zheng, J. L. Sonnenberg, M. Hada, M. Ehara, K. Toyota, R. Fukuda, J. Hasegawa, M. Ishida, T. Nakajima, Y. Honda, O. Kitao, H. Nakai, T. Vreven, J. A. Montgomery, Jr., J. E. Peralta, F. Ogliaro, M. Bearpark, J. J. Heyd, E. Brothers, K. N. Kudin, V. N. Staroverov, R. Kobayashi, J. Normand, K. Raghavachari, A. Rendell, J. C. Burant, S. S. Iyengar, J. Tomasi, M. Cossi, N. Rega, N. J. Millam, M. Klene, J. E. Knox, J. B. Cross, V. Bakken, C. Adamo, J. Jaramillo, R. Gomperts, R. E. Stratmann, O. Yazyev, A. J. Austin, R. Cammi, C. Pomelli, J. W. Ochterski, R. L. Martin, K. Morokuma, V. G. Zakrzewski, G. A. Voth, P. Salvador, J. J. Dannenberg, S. Dapprich, A. D. Daniels, Oe. Farkas, J. B. Foresman, J. V. Ortiz, J. Cioslowski and D. J. Fox, Gaussian 09, Revision A.2 2009, Gaussian, Inc., Wallingford CT.
55. C. Lee, W. Yang and R. G. Parr, *Phys. Rev. B: Condens. Matter*, 1988, **37**, 785-789.
56. A. D. Becke, *J. Chem. Phys.*, 1993, **98**, 5648-5652.
57. R. Krishnan, J. S. Binkley, R. Seeger and J. A. Pople, *J. Chem. Phys.*, 1980, **72**, 650-654.
58. Bruker Analytical X-ray Instruments, Inc., Madinson, WI, USA: SAINT and SADABS 2008.
59. L. Palatinus and G. Chapuis, *J. Appl. Crystallogr.*, 2007, **40**, 786-790.
60. V. Petříček, M. Dušek, L. Palatinus, 2006: Jana2006. The crystallographic computing system. Institute of Physics, Praha, Czech Republic.